

Discrete Porosity Method for Roughness Modelling in the Framework of RANS

Duc Duong Viet, Jitendra Kumar, Frank-Hendrik Wurm

Institute of Turbomachinery, University of Rostock
Albert-Einstein-Straße 2, Rostock, Germany

duc.viet@uni-rostock.de; jitendra.kumar@uni-rostock.de; hendrik.wurm@uni-rostock.de

Abstract - For various turbomachines, significant difference in calculated efficiency between CFD simulations and experiments is observed due to inappropriate wall-treatment methods for rough surfaces. A discrete porosity method is presented in this paper for roughness modelling in comparison to body-conforming mesh and equivalent sand-grain (ESG) roughness height. A physical dimension of each roughness elements are considered for simulation without creating conformal mesh for the rough surfaces. The roughness elements are defined as porous media with defined porosity factors according to Darcy-Forchheimer equations in OpenFOAM solver. This methodology is compared and validated to body-conforming RANS simulation results, where the roughness elements are designed as spanwise bars. The discrete porosity approach needs much lesser pre-processing effort than body-conforming mesh method, but the flow fields looks similar for both approaches. Moreover, the developed porosity method is applied for a realistic rough surface of the cast iron part which is obtained by confocal microscopy scanning method. The shift in maximum velocity because of one sided rough wall, and the difference in smooth and rough side turbulent Reynolds numbers are thoroughly presented. Additionally, the ESG height k_s^+ is calculated, to depict the influence of the roughness on the logarithmic law.

Keywords: porosity method, wall roughness, body-conforming mesh, RANS, rough channel, OpenFOAM

1. Introduction

Numerical simulations reduces the development cost of industrial products significantly. Therefore, numerical simulation results using computational fluid dynamics (CFD) methods must be reliable for the flow prediction. In many applications, CFD simulations are calculating accurate results regarding local flow field variables. However, there are some deficits. For example, the calculated efficiency of centrifugal pumps with low specific speed using CFD varies significantly from experiments. This is caused by improper wall treatment for rough surfaces [1].

Initially, Nikuradse proposed the idea of equivalent sand-grain (ESG) roughness height to modify logarithmic wall function for rough walls [2]. Later, Schlichting [3] demonstrated the influence of roughness shape and distribution density on ESG roughness height. After that, several correlation parameters are proposed to predict ESG roughness height [4]. But Taylor showed that predicted ESG roughness height could differ by 100 % from experimentally measured value [5]. Moreover, experimental data is needed for random-roughness to predict skin friction and heat transfer. Additionally, Busse et al. [6] also observed the drag dependence on surface topographical features in their DNS simulation for open-channel flow by using latest numerical simulation tools. Flack and Schultz [7] proposed latest correlation based on the root-mean-square roughness height and the skewness of the roughness probability density function for ESG roughness height prediction. But still, it doesn't fit for all types of roughness. The performance of slope-based correlations was verified by Yuan and Piomelli [8], and they showed that 'critical effective slope' is much higher for separating the waviness and roughness regimes. Even ESG roughness height model has limitations, but it is still established state of the art for roughness modelling in industrial applications.

A body-conforming mesh over rough surface in RANS/LES framework requires high computational power. In the case of high roughness features, body-conforming mesh generation is impossible. Discrete-element method (DEM) is an alternative technique for roughness model where the governing equation is modified by multiplying form-drag term and blockage fraction. Bons et al. [9] compared body-conforming RANS model, ESG roughness model and DEM numerical results to experimental results regarding skin friction and heat transfer for fuel-deposit and erosion-surface. It was shown

that deviation from experimental data is high for large roughness features for DEM model and ESG roughness model. Body-conforming fine-mesh with RANS equations were nearest to experimental data. Thus, exact geometrical representation of roughness element is better than ESG roughness model shifting the logarithmic law.

A scope for better roughness modelling technique in RANS framework is still open, which must include exact roughness geometry, but reduces the limitation of body-conforming mesh method regarding its need of high computational power.

Discrete-porosity method is a novel idea for roughness modelling, which resolves the flow near the wall and the roughness elements themselves. A sink term is added in momentum equation to discretized roughness element in the CFD simulation. It contributes porous properties to selected cells according to Darcy-Forchheimer equations described in the following section. Afterwards, a comparison between unsteady RANS simulation with body-conforming mesh and porosity model is carried out to validate this method. Then, a general application is presented, especially a simulation with a cast iron surface is described in detail. In the end, conclusions are drawn and possible future work is proposed.

2. Governing Equations and Methodology

2.1. Navier-Stokes Equations

The Navier-Stokes equations are the fundamental equations for CFD, next to the continuity and energy equation. Navier-Stokes equations are derived from the momentum equations in which the material properties are added:

$$\frac{\partial \rho u_i}{\partial t} + \frac{\partial \rho u_i u_j}{\partial x_j} = \frac{dp}{dx_i} + \mu \left[\left(\frac{\partial u_i}{\partial x_j} + \frac{\partial u_j}{\partial x_i} \right) - \frac{2}{3} \delta_{ij} \left(\frac{\partial u_i}{\partial x_i} \right) \right] + k_i \quad (1)$$

where $\frac{\partial \rho u_i}{\partial t}$ represents the time dependent term, $\frac{\partial \rho u_i u_j}{\partial x_j}$ the convective and $\mu \left[\left(\frac{\partial u_i}{\partial x_j} + \frac{\partial u_j}{\partial x_i} \right) - \frac{2}{3} \delta_{ij} \left(\frac{\partial u_i}{\partial x_i} \right) \right]$ the diffusive term. $\frac{dp}{dx_i}$ and k_i are the pressure term and external volume forces, respectively. With the continuity equation, Eq. (1) can describe every type of isothermal flow, providing the static pressure and three velocity components in a 3D system.

For the description of porosity, an additional sink term S is added to Eq. (1):

$$\frac{\partial \rho u_i}{\partial t} + \frac{\partial \rho u_i u_j}{\partial x_j} = \frac{dp}{dx_i} + \mu \left[\left(\frac{\partial u_i}{\partial x_j} + \frac{\partial u_j}{\partial x_i} \right) - \frac{2}{3} \delta_{ij} \left(\frac{\partial u_i}{\partial x_i} \right) \right] + k_i - S \quad (2)$$

This porosity method is originally used to simulate flows through porous media like sediments [11] or heat exchangers [10].

2.2. Darcy-Forchheimer Equations

The sink term described in Eq. (2) is considered as additional pressure drop. A relation between pressure drop over a specific length L and the mean velocity was derived by Darcy in his experiments. He has defined a linear behaviour with hydraulic conductivity k_h [11]:

$$\frac{\Delta p}{L} = \frac{1}{k_h} u \quad (3)$$

An improved expression known as the Darcy-Forchheimer equations is shown in Eq. (4) [10, 14]. The pressure drop is divided into a viscous term, which is linearly dependent on the velocity and an inertial term, which is dependent on the velocity square. These relations can also be seen as friction drag and form drag respectively. Here, \mathbf{u} is the velocity vector for a three dimensional domain. In the Darcy-Forchheimer equations, it is possible to define different porous properties in each flow direction. Thus, anisotropic behaviour can be considered, if necessary:

$$\mathbf{S} = \mu \mathbf{D} \mathbf{u} + \frac{\rho}{2} \mathbf{F} \mathbf{u} |\mathbf{u}| \quad (4)$$

$$\mathbf{S} = \begin{pmatrix} \frac{\partial p}{\partial x} \\ \frac{\partial p}{\partial y} \\ \frac{\partial p}{\partial z} \end{pmatrix}, \quad \mathbf{D} = \begin{pmatrix} D_{xx} & D_{xy} & D_{xz} \\ D_{yx} & D_{yy} & D_{yz} \\ D_{zx} & D_{zy} & D_{zz} \end{pmatrix}, \quad \mathbf{F} = \begin{pmatrix} F_{xx} & F_{xy} & F_{xz} \\ F_{yx} & F_{yy} & F_{yz} \\ F_{zx} & F_{zy} & F_{zz} \end{pmatrix} \quad (5)$$

2.3. Methodology for Roughness Consideration

Initially, a Cartesian grid is generated for the simulation of a rough channel without considering the roughness features as displayed in Fig. 1. Thus, the mesh quality regarding minimum angle, maximum aspect ratio and skewness of grid elements was reached 90° , 20 and 1 respectively. Then, a MATLAB script was written to read STL data of a rough surface (see Fig. 2) and the roughness height distribution was calculated by another efficient MATLAB code as shown in Fig. 3. The qualitative comparison of calculated roughness distribution and actual roughness geometry is presented in Fig. 4. The accuracy can be improved by increasing grid lines in MATLAB codes. The full Cartesian domain is divided into two sub-domains using roughness height distribution files in OpenFOAM (see Fig. 5). The upper sub-domain consists of fluid cell volumes and the other one is filled with roughness cell volumes. For fluid cell volumes RANS equations are used without any sink or source term. The porosity property according to Eq. (4) is defined for the roughness cell volumes. High values for Darcy and Forchheimer coefficients \mathbf{D} and \mathbf{F} are defined, so the flow will be completely blocked in this region.

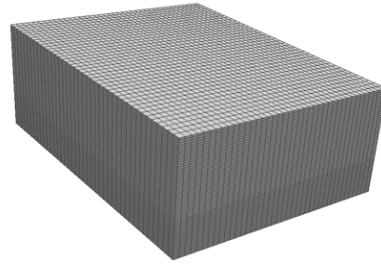


Fig. 1: Cartesian grid of a channel.

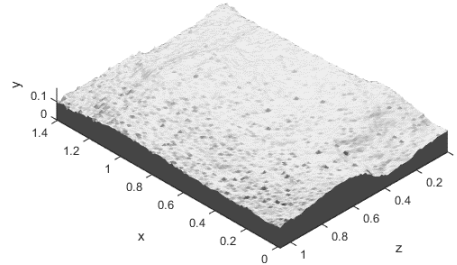


Fig. 2: STL data of rough surface.

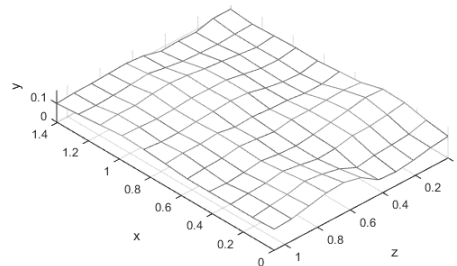


Fig. 3: Roughness height distribution using MATLAB code.

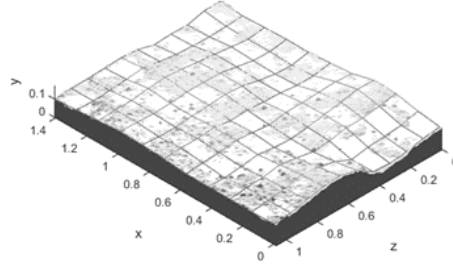


Fig. 4: Qualitative comparison of STL data to estimated roughness distribution.

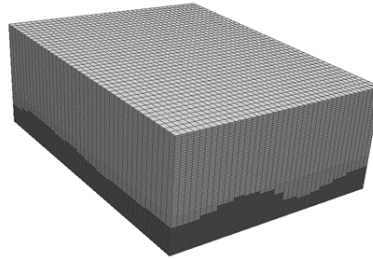


Fig. 5: Dividing a full Cartesian grid into two subdomain.

Here, a cell volume is either fluid cell volume or roughness cell volume. This leads to a difference in actual roughness geometry and mapped roughness zone in Cartesian grid. A simple two dimensional sketch is drawn to explain this issue as depicted in Fig. 6. The white cells are fluid cells, for which the continuity and Navier-Stokes equations are solved. The black line symbolizes the actual surface roughness and in dark grey the roughness cells are shown, for which the flow is blocked by defining porosity property. It is observed that some cells are selected as a roughness cell volume even roughness distribution is having very small volume fraction or vice versa (see Fig. 6 (left)). This discrepancy must be resolved for better simulation results. For a more reliable simulation, an improvement of this method can be seen in Fig. 6 (right). Here, the roughness cell volumes are again subdivided in a part which fully blocks the flow (dark grey) and other part which is partially blocked (grey) as shown in Fig. 6 (right) using MATLAB code. These cells are located between the fluid and the solid cells and are treated as a porous layer, so that the Darcy-Forchheimer coefficients have not a high value, but a value which should be a function of the volume fraction between fluid and solid.

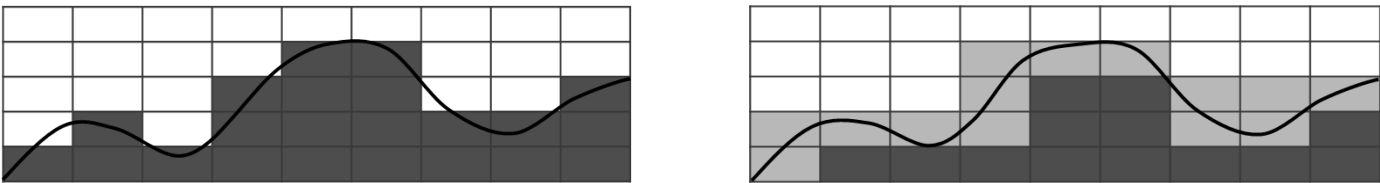


Fig. 6: Schematic representation of roughness elements (dark grey), fluid elements (white) and actual roughness contour (black) on left side; subdivision of roughness consideration in fully solid elements (dark grey) and porous elements (grey) on right side.

3. Validation of Porosity Method

For the validation of the porosity method, the model is compared to the experimental results and DNS simulation of a one sided rough wall channel [16]. Transverse square bars oriented in spanwise direction are mounted on one side of the channel. The channel dimensions are defined as $8H \times 2H \times 3H$ in x-, y-, z- direction respectively, where $H = 0.02 \text{ mm}$ is the half channel width. The square bars have an edge length of $k = 0.1 H$ and a distance of $\lambda = 4 k$ from each other. The roughness dimensions are summarized in Fig. 7. The grid of body-conforming mesh (Fig. 8) is generated sufficiently fine to reach $y^+ < 1$. The grid for porosity method (Fig. 9) is defined in a manner that roughness geometry is not intersecting to any cell volumes. Thus, no cell volume is needed to define as partial fluid volume or partial roughness volume.

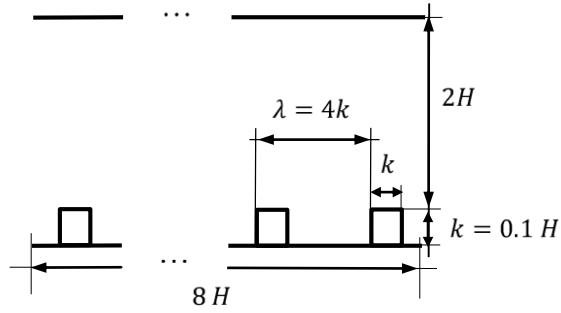


Fig. 7: Definition of channel and roughness dimensions.

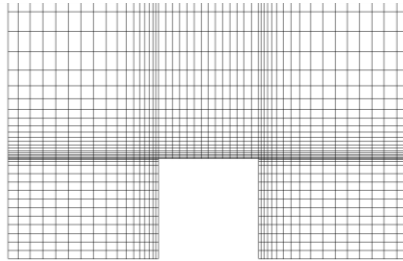


Fig. 8: Hex grid for body-conforming mesh.

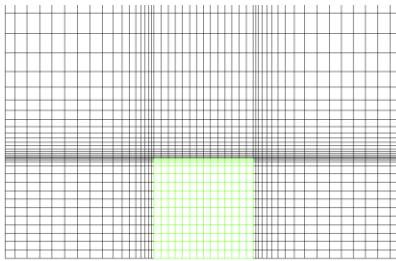


Fig. 9: Hex grid for porosity approach.

The simulations had been carried out at $Re = 2800$ and compared to experimental and DNS data. Because of the one sided roughness, the position of maximum velocity is not at the centre line of the channel, but is shifted towards the smooth channel side. The position y_u of maximum velocities is normalized by the half channel height H . For the assigned Reynolds numbers the velocity shift is $y_{U_{Burattini}} = 1.22 H$.

In Fig. 10, a comparison is shown regarding the velocity profile between Burattini [16], the body conforming simulation and the porosity method at $Re = 2800$. The simulations of body conforming and porosity method has been carried out in the framework of unsteady RANS with the $k - \omega - SST$ turbulence model. The result of body conforming mesh comes closer to the result of the paper from Burattini than the porosity model. The shift of the maximum velocity from the centre is $y_{U_{BC}} = 1.16 H$ for the body conforming simulation. For the porosity method, a shift of $y_{U_{porous}} = 1.47 H$ occurs, which is higher than from Burattini $y_{U_{Burattini}} = 1.22 H$. Moreover, the contour of the velocity profiles themselves differ both from the results of [16]. In the first half of the channel, where $y/H < 1$, the velocity reduction caused by the roughness elements is underestimated by the body conforming and overestimated by the porosity method. In the second half where $y/H > 1$, the velocity contour behaves the other way round because of the different behaviours in the first channel half and the different maximum velocity shifts.

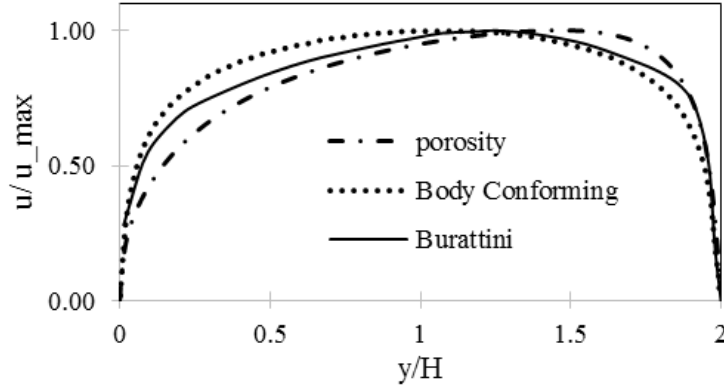


Fig. 10: Comparison of velocity profiles; - - - porosity method, body conforming mesh simulation, — Burattini [16] at $Re = 2800$.

The reason for the disparity in results of body conforming and porosity method lies in the velocity gradient at the wall of the roughness elements. In body conforming method, the faces of the roughness elements are considered as patches which are treated as walls with no slip condition. This is standard procedure for wall boundary condition, and $y^+ < 1$, so the viscous sublayer is fully resolved. Same mesh is used for porosity method, so the resolution is adequate. Considering the roughness elements, they are treated in a way, in which the velocity is decreased by a sink as described in Eq. (4). Inside the roughness elements, the velocity reaches to a value close to zero with values in dimension of $10^{-5} m/s$. At the threshold between fluid and solid, the sink seems to be less effective. Therefore, the velocity becomes a value less close to zero. Consequently, the velocity gradient at the wall of the roughness element becomes smaller, compared to body conforming simulation. This leads not only to the difference in velocity profile, but also to different wall shear stress, friction velocity and in the end to different k^+ as shown in Table 1.

Table 1: Comparison of flow field data.

	Burattini [16]	Body Conforming Mesh	Porosity Method
u_{τ_r}/u_{max}	0.073	0.0765	0.0542
Re_{τ_r}	260	259	192
Re_{τ_s}	190	192	221
$y_{u_{max}}/H$	1.22	1.16	1.47
k^+	26	25.9	19.2

It is observed that body-conforming simulation giving flow data nearest to the experimental data performed by Burattini. Therefore, to compare approaches for ESG height, body-conforming results are considered as references. ESG height for body-conforming simulations, porosity method and correlation according to Sigal and Danberg [20] are 0.66, 0.72 and 1.4 [mm], respectively. Thus, porosity method proves its potential for roughness estimation over empirical ESG approach. Now, porosity method is extended for realistic surface for general applications.

4. Discrete porosity method for realistic surface

The simulations using porosity approach is extended for realistic cast iron surface. Because in the case, some cell volume will have definitely partial fluid zone or roughness zones as shown in Fig. 6 (right). For these type of cell volumes the sink term is modified and written as Eq. 6, where α is considered as volume percentage of solid in local fluid cell volumes.

$$S = \alpha\mu Du + \alpha \frac{\rho}{2} Fu|u| \quad (6)$$

The simulation domain has the dimensions of $8H \times 2H \times 3H$ in x -, y - and z -direction, respectively, but with half channel height of $H = 0.005 \text{ m}$. The reduced channel height has been chosen, because the mean roughness height of cast iron takes only 0.1196 mm and the maximum height 0.1675 mm . Besides, the area of the cast iron with $1.4208 \text{ mm} \times 1.0653 \text{ mm}$ cannot fill the whole domain. Therefore, this cast iron part was mirrored in span- and streamwise direction, so that it fits 14 times in spanwise and 28 times in streamwise direction into the domain. Moreover, the ratio between boundary layer thickness and mean roughness height is $\delta/k = 41.8$. According to Flack and Schultz, the boundary layer thickness should be much greater than the roughness height [17, 18]. This is valid for this case, because the ratio is between 16 and 110 [18]. The ratio of boundary layer thickness and roughness height in Burattini et. al. [16] was even $\delta/k = 10$.

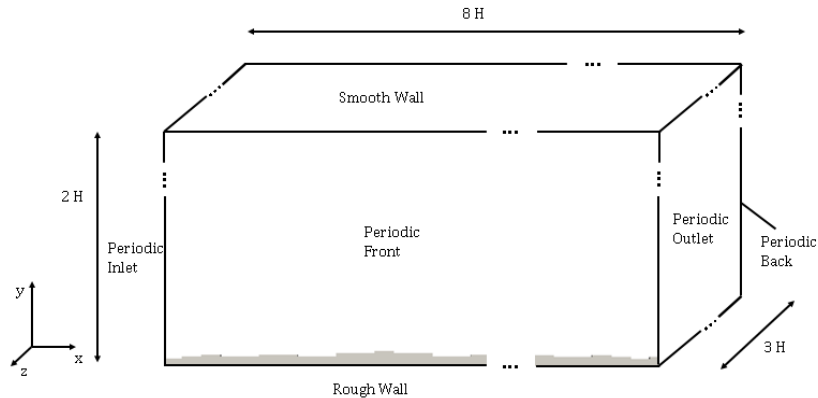


Fig. 11: Channel dimension and boundary condition for simulation of cast iron.

For reliable simulation, a mesh study was carried out for the simulation of the roughness consideration, in which the layer between fluid and solid works as a porous layer, while the solid layer is blocking the flow fully. The 5.9 million nodes were selected for comprehensive simulations. Bulk Reynolds numbers of 3000 and 7000 were chosen with a channel height of $2H = 0.01 \text{ mm}$ and water with kinematic viscosity of 10^{-6} . Periodic boundary conditions were set in span- and streamwise direction, see Fig. 11, with a pressure gradient in to maintain the bulk velocity of 0.3 m/s and 0.7 m/s in streamwise direction for the respective Reynolds numbers.

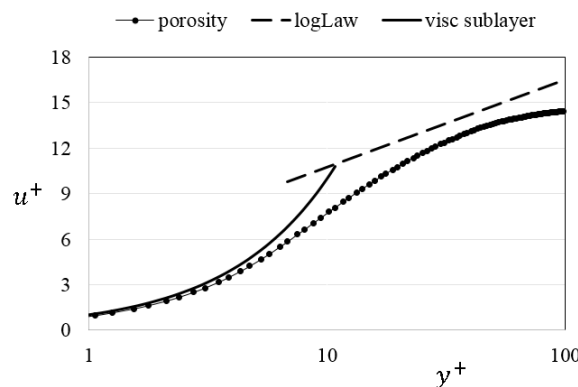


Fig. 12: Comparison of logarithmic wall behavior of flow on smooth side of wall at $Re_b = 3000$ with analytical wall function.

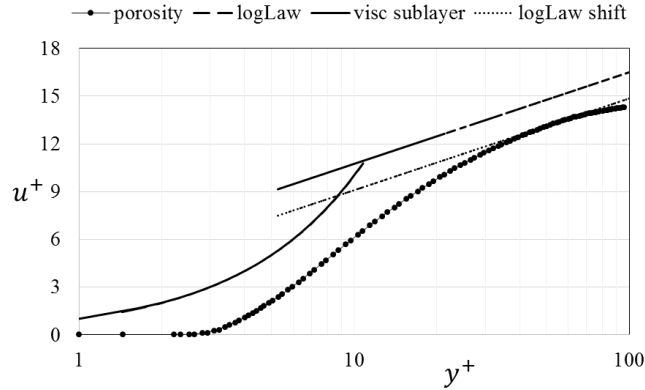


Fig. 13: Comparison of logarithmic wall behavior of flow on rough side of wall at $Re_b = 3000$ with analytical wall function.

At smooth wall, the viscous sublayer of the simulation matches well with the analytical function until around $y^+ = 5$ as depicted in plot Fig. 12. Afterwards, the results are showing the buffer layer which is the threshold between viscous sublayer and logarithmic layer. In the logarithmic region, the results from the simulation are slightly lower than the analytical function, they come closest in a small range $30 < y^+ < 55$. Because of the relatively small Reynolds number of 3000, the viscous sublayer and the buffer layer are already ranging far into the channel center. Moreover, the maximum velocity is shifted to the smooth channel side. Therefore, $y^+ = 100$ has already nearly reached the position of maximum velocity. At higher Reynolds number, the logarithmic region should fit better to the analytical function. A similar behavior of the rough side can be noticed compared to the smooth side regarding viscous sublayer, buffer layer and logarithmic layer. The complete curve is shifted downwards as shown in Fig. 13, which is the typical influence of roughness on the wall.

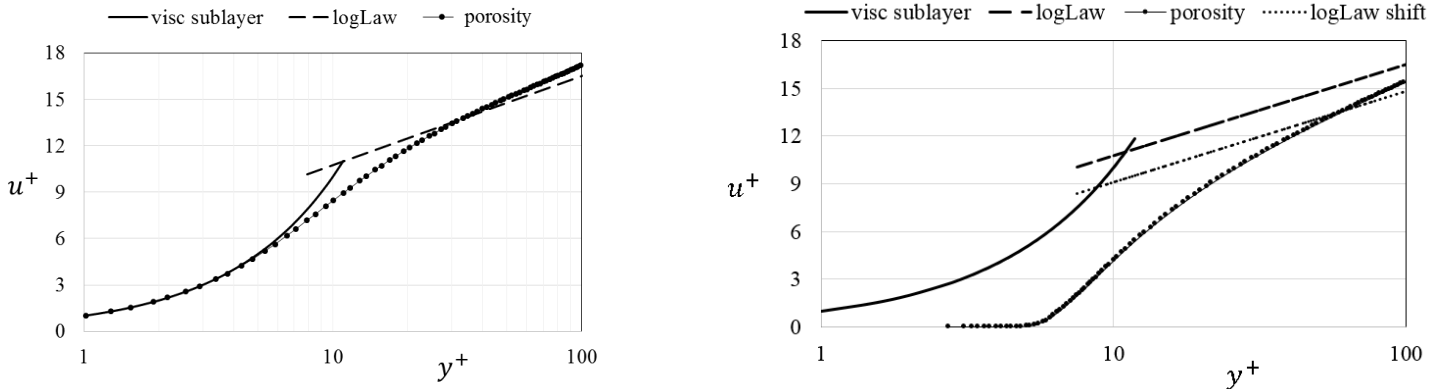


Fig. 14: Comparison of logarithmic wall behavior of flow at $Re_b = 7000$ with analytical wall function on smooth surface (left) and rough surface (right).

Another simulation with the same setup has been carried out, but at Reynolds number of 7000. The results are shown in Fig. 14. In contrast to the simulation at $Re = 3000$, the values of u^+ intersect the analytical function in the logarithmic region. So, the slope of the simulation results is higher than in the analytical logarithmic law, which is caused by an underestimated velocity gradient. This is consistent to the statement figured out when validating the porosity method in section 3. Validation of numerical results are planned by in-house experimental analysis of selected rough channel.

Conclusion

The porosity method has strong potential for CFD simulations with appropriate roughness treatment. An enormous computational effort can be reduced by this proposed method even geometry of roughness element is considered. For the square bar roughness, the equivalent sand-grain height based on porosity method and Sigal and Danberg correlation differ from body-conforming simulation results by 8% and 112%, respectively.

This method is extended for realistic surfaces and sink term is defined for each cell volumes based on volume percentage of solid in the local cell volumes. An efficient MATLAB script is written to divide full Cartesian mesh into fluid domain, pure roughness zones and partial roughness zones. Moreover, additional function is added to script to calculate volume fraction of solid for the partial roughness zone. Thus this method is distinguished as ‘discrete porosity method’. For general application, a cast iron surface given as STL-file has been applied on one side of a channel and is simulated in OpenFOAM at $Re_b = 3000$ and $Re_b = 7000$. Detailed results is presented in this paper. Additionally, the near wall behaviour of the simulation has been compared to the analytical functions of viscous sublayer and logarithmic wall function.

It is observed that the velocity profile at roughness element is not properly resolved because of insufficient no slip condition. Moreover, only volume fraction of roughness is considered to modify sink term but slope of roughness element must be included in the equations. Nevertheless, experimental validation of the method is always needed. So these two task are considered as future work.

References

- [1] K. Juckelandt, “Applicability of wall-function approach in simulations of turbomachines,” in *Proceedings of ASME Turbo Expo 2015: Turbine Technical Conference and Exposition GT 2015*, Canada, GT2015-42014, 2015.
- [2] J. Nikuradse, “Laws of flow in rough pipes,” *NACA Technical Memorandum 1292*, Washington, 1950.
- [3] H. Schlichting, “Experimental investigation of the problem of surface roughness,” *NACA Technical Memorandum 823*, Washington, 1937.
- [4] R. L. Simpson, “A Generalized Correlation of Roughness Density Effects in the Turbulent Boundary Layer,” *AIAA J.*, vol. 11, no. 2, pp. 242-244, 1973.
- [5] R. P. Taylor, W. F. Scaggs, and H. W. Coleman, “Measurement and Prediction of the Effects of Nonuniform Surface Roughness on Turbulent Flow Friction Coefficients,” *ASME J. Fluids Eng.*, vol. 110, pp. 380-384, 1988.
- [6] A. Busse, M. Lütznier, and N. D. Sandham, “Direct numerical simulation of turbulent flow over a rough surface based on a surface scan,” *Comput. FLUIDS*, vol. 116, pp. 129-147, 2015.
- [7] K. A. Flack and M. P. Schultz, “Review of Hydraulic Roughness Scales in the Fully Rough Regime,” *J. Fluids Eng.*, vol. 132, 2010.
- [8] J. Yuan and U. Piomelli, “Estimation and prediction of the roughness function on realistic surfaces,” *J. Turbul.*, vol. 15, no. 6, pp. 350-365, 2014.
- [9] J. P. Bons, S. T. McClain, Z. J. Wang, X. Chi, and T. I. Shih, “A Comparison of Approximate Versus Exact Geometrical Representations of Roughness for CFD Calculations of C_f and St ,” *J. Turbomach.*, vol. 130, no. 021024, pp. 1-10, 2008.
- [10] D. Missiris, S. Donnerhack, O. Seite, C. Albanakis, A. Sideridis, K. Yakinthos, A. Goulas, “Numerical development of a heat transfer and pressure drop porosity model for a heat exchanger for aero engine applications,” *J. Applied Thermal Eng.*, vol. 30, pp. 1341-1350, 2010.
- [11] H. Darcy, “Les fontaines publiques de la ville de Dyon,” Paris, Victor Dalmont, 1856.
- [12] A. Hazen, “Some physical properties of sand and gravels with special reference to their use in filtration,” Massachusetts State Board of Health, Twenty-fourth annual report 541, 1893.
- [13] K. Boomsma, D. Poulikakos, “The effects of compression and pore size variations in a liquid flow characteristics of metal foam,” *J. Fluids, Engineering Transactions of the ASME*, vol. 124, pp. 263-272.
- [14] A. J. D. J. Dupuit, “Etudes Theoriques et Pratiques sur le mouvement des aux dans les canaux decouverts et a travers les terrains permeables,” Paris, Victor Dalmont, 1963.
- [15] I. Newton, “Philosophiae Naturalis Principia Mathematica,” The Principal, Prometheus Books, New York, 1687.
- [16] P. Burattini, S. Leonardi, P. Orlandi and R. A. Antonia, “Comparison between experiments and direct numerical simulations in a channel flow with roughness on one wall,” *J. Fluid Mech.*, vol. 600, pp.403-426, 2008

- [17] K. A. Flack, M. P. Schultz and T. A. Shapiro, "Experimental support for Townsend's Reynolds number similarity hypothesis on rough walls," *Physics of Fluids*, vol. 17, p. 035102, 2005.
- [18] K. A. Flack, M. P. Schultz and J. S. Connely, "Examination of a critical roughness height for outer layer similarity," *Physics of Fluids*, vol. 19, p. 095104, 2007.
- [19] H. Schlichting, *Boundary Layer Theory*. Berlin, Springer, 2003.
- [20] A. Sigal, J. E. Danberg, "New Correlation of Roughness Density Effect on the Turbulent Boundary Layer," *AIAA Journal*, vol. 28, no. 3, pp. 554-556, 1989.